Randomness-Based Scale-Chromatic Image Analysis for Interactive Mapping on Satellite-Roadway-Vehicle Network

Kohji Kamejima

Faculty of Information Science and Technology, Osaka Institute of Technology
1-79-1 Kitayama, Hirakata 573-0196 JAPAN

ABSTRACT

A new framework is presented for integrating satellite/avionics sensors with onboard vision to support information intensive maneuvering. Real time bindings of the bird's eye observation and the driver's view via GPS provides *as-is* basis for perception and decision. Randomness-based roadway pattern model is implemented by fractal coding scheme associating bird's eye and frontal views. The feasibility of the framework with resquirements for vison system is discussed through concept modeling and experimental studies.

Keywords: Interactive Mapping, Multi-Viewpoint Image, Randomness-based Image Analysis, Fractal Pattern Coding, Natural Complexity

1 INTRODUCTORY REMARKS

Via two decades of investigations intended for autonomous mobile robots [19], [18], it has been demonstrated that the essential capability for maneuvering arises from location specific integration of multi-viewpoint imagery. In fact, site-route graph associated with landmark views as shown in Fig. 1 provides the prediction of scene to be matched [14]. By applying search algorithms to graph structure, associated roadway pattern can be extracted. The introduction of inter-pattern kinetics completes autonomous maneuvering process as a computer implementation of perceptual cycle [16]. The concept of information intensive maneuvering was extended to vehicle-highway integration intended for interactive support of joint perception-decision processes [13].

Computational access of maneuvering process to the site-route description requires essentially symbolic model consisting of finite landmark objects. As a physical entity, behavior of individual vehicle should be situated relative to the landmark objects. To integrate computational-geometric decisions, current navigation systems are configured on 'digital map' where the totality of geographical information is *a priori* packaged.

On the basis of site-route structure, we can reconstruct key technologies of robot vision to realize interactive decision support systems. To this end, the site-route representation should be updated interactively [17]. In this interactive mapping process, vision system accepts human's pointing on scene image to locate the object in well-structured digital map. Due to essential discrepancy in representation levels of well-structured symbol system and naturally complex scene, however, the matching of the digital map with real scene is left to high-level understanding by human spatial intelligence [2]. Furthermore, decision processes for updating and customizing the digital map on ceaselessly varying 'real' scene easily fall into computational explosion within the framework of conventional closed-logic machine [12].

Hence, it is not easy for robot vision to support human's perception and decision. In this paper, the concept of interactive mapping is re-structured within the context of information intensive transportation. Basic

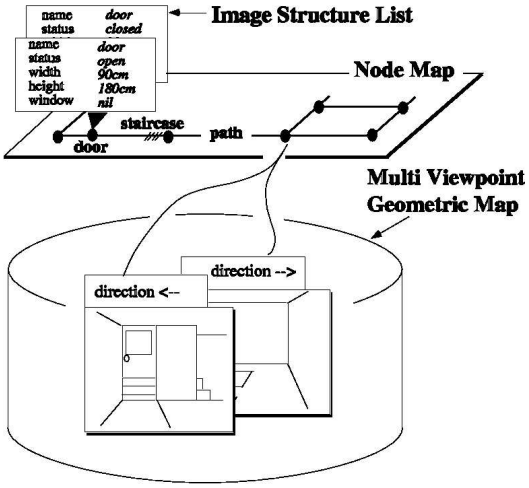

Figure 1: Multi Viewpoint Site-Route Map

On route representation in terms of node-path chain, maneuvering process is symbolically computable. In accordance with continuous positioning, multi-viewpoint map provides geometric descriptions of landmark objects attached at the next node. Vision system, then, matches the perspectives of landmark objects with dynamically varying view of physical world.

Figure 2: Aerial Photograph as *as-is* Map

Advancements in remote sensing and precise imaging technology make it possible to capture as-is geometry of terrain. By applying robot vision for 'reading' roadway patterns in such bird's eye images, exact digital map is generated automatically. Images from multi viewpoint observation are integrated on today's information network to support human's decision in the scene.

idea is to coordinate robot vision and human perception through decentralized access to common digital map. As the basis of mapping processes, in what follows, images captured by onboard camera and satellite sensors are invoked as multi-viewpoint observation of the scene. In reference to the symbolic structure of *a priori* digital map, the multi view point imagery are identified as consistent aspects of really existing scene and integrated into a unified *as-is* map.

2 IN PROCESS MULTI-VIEWPOINT INTEGRATION

Recent advances in avionics and space technology open up new application of robot vision to sensing based implementation of the interactive mapping scheme. In this implementation, aerial photograph and/or remote sensing data as shown in Fig. 2 are introduced as the latest *as-is* representation of local terrain. In this *as-is* representation, roadway pattern is imaged exactly but corrupted by really existing background objects.

Today's global positioning system (GPS) is equipped with the capability for associating broadcasted bird's eye view with individually captured frontal view of the scene. Once the association is established, the vision system can trace the bird's eye imagery for predicting roadway pattern. In addition, mutual access to the bird's eye – frontal view bindings expands the horizon of individual vehicle to a community of maneuverers; histories of maneuvering processes by individual vehicles are gathered and extracted to capture 'blind' scene.

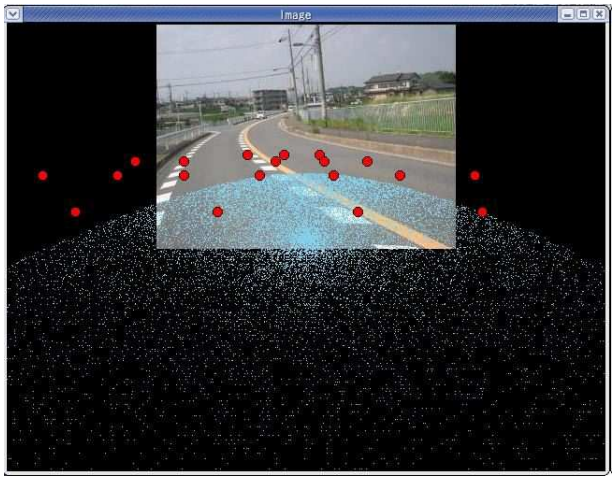

Figure 3: GPS Signal Mapped on a Frontal Image

Fluctuation of GPS data is marked by (•) and mapped in a scene image. As the results of various levels of error correction, positioning residual is confined in a small area. In this case, the deviation of positioning results is bounded by a circle covering a roadway.

To evaluate such cooperative expansion of decision space, typical examples of GPS information has been mapped on a scene image as shown in Fig. 3 [9]; though received signal is interpolated via Kalman filtering, approximately 0.1 sec. of longitude-latitude errors are remained. This implies that individual vehicle can be located with approximately ±3m drift. Dynamic behavior of GPS residuals is shown in Fig. 4. As shown in this figure, the GPS residual is triggered by random shower of X-ray (↑) from cosmos; the residual maintains nondeterministic drift without the X-ray burst. Through theoretical and experimental investigation of atmospherics, the main part of the drift has been modeled in terms of the 'ionosphere instability'; despite essential nonlinearity, the dynamics of the GPS residual is shown to be restored by using adaptive Kalman filter [11]. Thus, current version of GPS can be exploited to select a roadway in both bird's eye and frontal views as shown in figure 3. This implies that the satellite-roadway-vehicle linkage provides *in-situ* basis for perception and decision.

To extend the multi-viewpoint site-route map on the satellite-roadway-vehicle network, robot visions are required to be re-formulated; new problem is to recognize 'really existing objects' bearing complex view suffering from essentially unpredictable 'micro damages'. Through satellite sensors and onboard camera, such complexity can be captured as noisy reflections of daylight at the same objects. Despite intrinsic unpredictability, various levels of perception processes

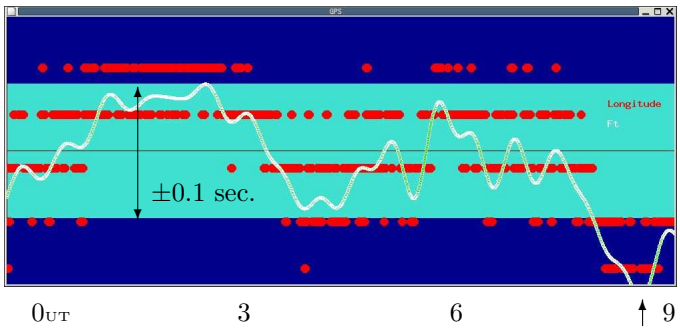

(a) Time Evolution of Longitude Residual

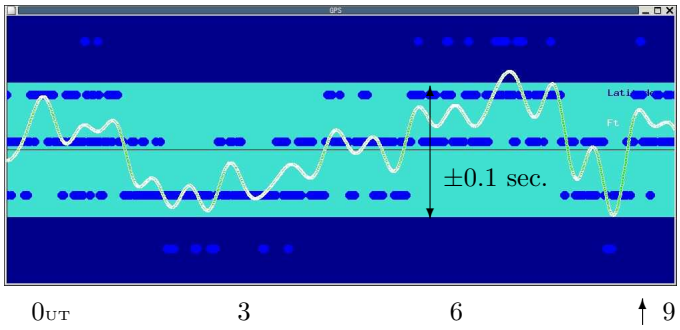

(b) Time Evolution of Latitude Residual

Figure 4: GPS Residual

GPS signal suffers from various types of disturbances added in signal transmission process. The fluctuation increases in response to random shower of X-ray from cosmos. By the nonlinearity of ionosphere dynamics, the time evolution of the residual exhibits limit cycles with period 10 – 20 min.

should be supervenient to the three-dimensionality of the objects [15]. In fact, early vision organizes skewed texture in optical flow *prior* to the reconstruction of object surfaces [3]. Simultaneously, it has been pointed out that human perception is sufficiently sensitive to the reflection of 'white daylight' even under considerable spectrum shift [4]. These facts imply that random texture of object specific coloring resulted from 3D 'roughness' of the surfaces *affords* crucial cues to activate early perception. Thus, the expansion of object surfaces can be restored through morpho-chromatic analysis of random reflections.

As an *as-is* part of unified real world, natural object maintains essentially unpredictable consistency within really existing 'background noise'. Such universal mechanisms stochastically governs the image of not-yet-identified objects. In what follows, generic representation of object specific randomness is represented by the combination of two kinds of universal imaging rules: chromatic diversity and self-similarity.

Let object be observed in terms of brightness distribution f in the image plane Ω. The universal rules, i.e., chromatic diversity and self-similarity can be associated with f via multi-scale and multi-spectral analysis [7], [10]. The existence and detectability of universal rules on the information (Ω, f), imply that natural randomness can be organized as *maneuvering affordance* to induce subsequent decision processes [8].

3 GENERIC PALETTE

Human vision can distinguish subtle chromatic variations using only three types of receptors. This implies that continuous variation of reflective spectral power can be articulated into 'trichromatic primaries.' On the other hand, physical aspect of coloring processes can be observed via the brightness distribution f. Due to geometric inconsistency, however, it is not easy to match coloring processes associated with natural objects precisely [7]. Noticing this, let the chromatic information conveyed by the distribution f be represented in the totality of 'positive' 3D vectors R^3_+:

$$f^{\mathtt{RGB}} \;=\; [\mathtt{R}\quad \mathtt{G}\quad \mathtt{B}]^T, \qquad \mathtt{R},\mathtt{G},\mathtt{B} \geq 0,$$

where $\mathtt{R}$, $\mathtt{G}$, $\mathtt{B}$ denote the intensity of primaries. Define

$$\phi(f^{\mathtt{RGB}}) \;=\; \frac{f^{\mathtt{RGB}}}{|f^{\mathtt{RGB}}|}, \tag{1}$$

with intensity distribution given by

$$|f^{\mathtt{RGB}}| \;=\; \sqrt{\mathtt{R}^2+\mathtt{G}^2+\mathtt{B}^2}.$$

By introducing Euclid norm $|f^{\mathtt{RGB}}|$ in stead of 'gay level' of conventional color representation systems, the discrepancy of coloring process can be exactly evaluated via geometric computation. In R^3_+, thus, we can separates chromatic information from the intensity $|f^{\mathtt{RGB}}|$ precisely.

For this purpose, consider the positive unit sphere

$$\Phi^{\mathtt{RGB}} \;=\; \Big\{\, \phi(f^{\mathtt{RGB}}) \in R^3_+ \;\Big|\; |\phi(f^{\mathtt{RGB}})| = 1 \,\Big\}, \tag{2}$$

called chromatic information space, and let the information $f^{\mathtt{RGB}}$ be mapped into $\Phi^{\mathtt{RGB}}$. In $\Phi^{\mathtt{RGB}}$, the consistency of trichromatic vectors

$$f_i^{\mathtt{RGB}}, f_j^{\mathtt{RGB}} \;\in\; R^3_+,$$

can be indexed in terms of the 'inner product'

$$\phi_i^T(f_i^{\mathtt{RGB}})\phi_j(f_j^{\mathtt{RGB}}).$$

In R^3_+, we have

$$\phi_i^T(f_i^{\mathtt{RGB}})\phi_j(f_j^{\mathtt{RGB}}) \;\geq\; 0. \tag{3}$$

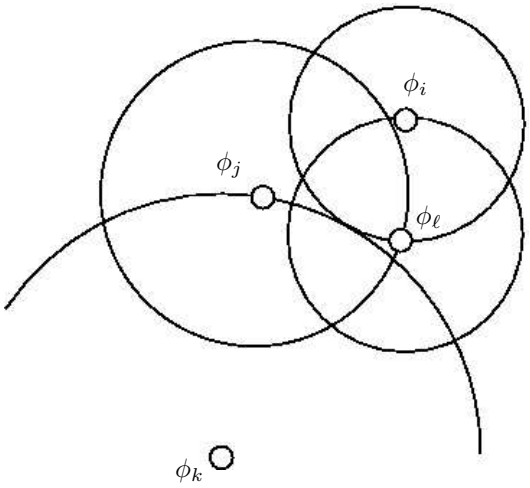

Figure 5: Palette of Samples

The chromatic consistency index induces a distance in Φ^{RGB}. The intersection of a positive vector ϕ_k with the unit sphere Φ^{RGB} is linked by that of ϕ_j with distance evaluation $g_{RGB}(\phi_k|\phi_j)$. The vectors ϕ_i and ϕ_ℓ are closely located with less distance $g_{RGB}(\phi_i|\phi_\ell) = g_{RGB}(\phi_\ell|\phi_i)$.

For such positive index, define

$$\theta_{ij} \quad = \quad \cos^{-1}(\phi_i^T \phi_j).$$

Noting the following estimate

$$\cos\theta_{ij} \sim \sqrt{1-\theta_{ij}^2} \quad \sim \quad e^{-\theta_{ij}^2/2},$$

for sufficiently small θ_{ij}, as well as the following evaluation

$$\theta_{ij} \quad \sim \quad |\phi_i - \phi_j|,$$

for sufficiently consistent chromatic information, we have

$$\frac{\phi_i^T \phi_j}{2\pi} \quad \sim \quad g_{\mathtt{RGB}}(\phi_i|\phi_j), \tag{4a}$$

where $g_{\mathtt{RGB}}(\phi_i|\phi_j)$ denotes 2D Gaussian probability density

$$g_{\mathtt{RGB}}(\phi_i|\phi_j) \quad = \quad \frac{1}{2\pi}\exp\left[-\frac{|\phi_i-\phi_j|^2}{2}\right]. \tag{4b}$$

The association (4) implies that the consistency index (3) induces the maximum entropy criterion in chromatic consistency analysis.

By invoking the measure $g_{\mathtt{RGB}}$, we can introduce a topology in $\Phi^{\mathtt{RGB}}$ as shown in Fig. 5. Let a set of chromatic information $\mathfrak{s} = \{\,\phi_i, i = 1, 2, \ldots, \|\mathfrak{s}\|\,\}$ with size $\|\mathfrak{s}\|$ be sampled as a 'palette' of object image and mapped into the chromatic information space $\Phi^{\mathtt{RGB}}$. The diversity of the palette is indexed in terms of the following measure:

$$\mathtt{R}_{\mathfrak{s}} \quad = \quad g_{\mathtt{RGB}}\left(-\frac{\sigma_{\phi\phi}}{2\alpha}\right), \tag{5a}$$

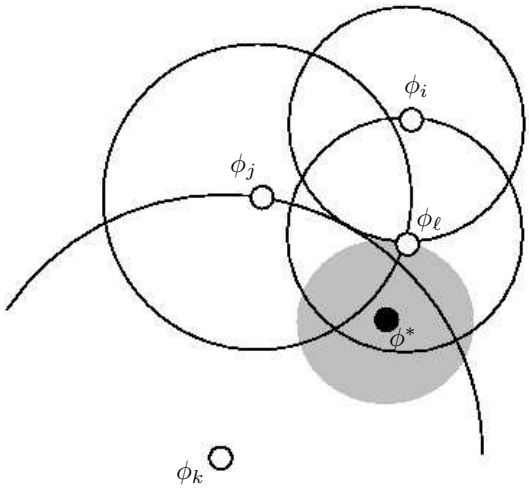

Figure 6: Matching with the Palette:

The unity of the vector set $\mathfrak{s} = \{\,\phi_i, \phi_j \ldots\}$ is indexed by the longest distance $g_{RGB}(\phi_k|\phi_j)$ whereas the identity as a 'palette' $\mathfrak{s}$ is evaluated in terms of the minimal distance $g_{RGB}(\phi_i|\phi_\ell)$. A new vector ϕ^* is included in the palette if the minimal distance $g_{RGB}(\phi^*|\phi_\ell)$ satisfies the condition given by (6).

where

$$\sigma_{\phi\phi}^2 \quad = \quad -\frac{2}{\|\mathfrak{s}\|(\|\mathfrak{s}\|-1)} \times \log\left[\prod_{\substack{1\le i,j\le\|\mathfrak{s}\| \\ i\neq j}} g_{\mathtt{RGB}}(\phi_i|\phi_j)\right]. \tag{5b}$$

In Eq. (5), $\mathtt{R}_{\mathfrak{s}}$ denotes the 'radius of paint' with respect to 'risk factor' α. By this $\mathtt{R}_{\mathfrak{s}}$, we can match observed chromatic information ϕ^* with the palette $\mathfrak{s}$ as follows:

$$g_{\mathtt{RGB}}(\phi^*|\mathfrak{s}) > \mathtt{R}_{\mathfrak{s}} \quad \Rightarrow \quad \phi^* \sim \mathfrak{s}. \tag{6}$$

where

$$g_{\mathtt{RGB}}(\phi^*|\mathfrak{s}) \quad = \quad \max_{\phi_j\in\mathfrak{s}} g_{\mathtt{RGB}}(\phi^*|\phi_j).$$

The schematics of this chromatic consistency evaluation is illustrated in Fig. 6. In this figure, the information ϕ^* and the 'nearest paint' $\phi_\ell \in \mathfrak{s}$ selectively matched with consistency $> \mathtt{R}_{\mathfrak{s}}$. The implication of the generic palette is demonstrated in Fig. 7; based on the pointing of the width and depth of the roadway (a), samples of coloring are collected via fractal covering (b); as the result of the matching of entire image with the palette generated by the coloring samples, the expansion of roadway is extracted (c).

4 GENERIC PATTERN

Let $\mathcal{F}[\Omega]$ be the totality of subsets of Ω and consider 2D dynamical system driven by contraction mappings

(a) Specification of Width and Depth

(b) Fractal Sampling

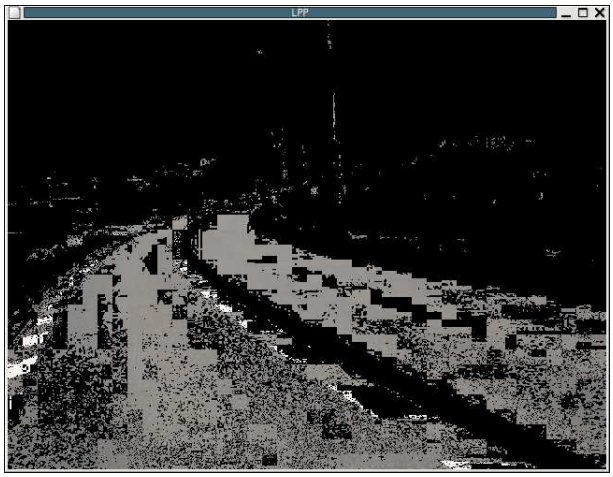

(c) Extracted Consistent Domain

Figure 7: Complex Pattern Extraction

As-is roadway pattern is extracted in the scene image via palette matching. Fractal imaging process generates random samples for covering target area efficiently.

$\mu_i : \Omega \mapsto \Omega$ where μ_i is randomly selected from fixed set of contraction mappings $\nu = \{\, \mu_i \,\}$:

$$\xi_{t+1} \quad = \quad \mu_i(\xi_t). \tag{7}$$

Following the theory of iterated function system (IFS) [1], the snapshots of random walk ξ_t, $t = 1, 2, \ldots$, are accumulated in a image plane Ω to generate a measure $\chi^{\mathfrak{p}}_{\Xi}$. It is known that the self-similarity process (7) generates a fractal attractor if the mapping set ν satisfies the open set condition [5]. In spite of geometric singularity of such an attractor, resulted measure $\chi^{\mathfrak{p}}_{\Xi}$ on $\mathcal{F}[\Omega]$ visualizes exactly the information of complex imaging process (7). In fact, the measure $\chi^{\mathfrak{p}}_{\Xi}$ is identified with a 'gray-level distribution' which is invariant in the following sense [1]:

$$\chi^{\mathfrak{p}}_{\Xi}(\Lambda) \quad = \quad \sum_{\mu_i \in \hat{\nu}} p_i \chi^{\mathfrak{p}}_{\Xi}[\mu_i^{-1}(\Lambda)], \tag{8}$$

for arbitrary $\Lambda \in \mathcal{F}[\Omega]$. In equation (8), p_i denotes the probability for selecting μ_i from ν. Since the 'non-zero area' of the invariant measure specifies complex pattern satisfying the self-similarity

$$\Xi \quad = \quad \bigcup_{\mu_i \in \nu} \mu_i(\Xi), \tag{9}$$

we can exploit $\chi^{\mathfrak{p}}_{\Xi}$ as a version of the probability for detecting complex patterns. Due to infinite resolution of the attractor Ξ, it is not easy to analyze resulted measure $\chi^{\mathfrak{p}}_{\Xi}$ as 'imagery'. This computational difficulty has been eliminated by introducing 'capturing probability' $\varphi(\omega|\nu)$ which is generated as smooth image via the following diffusion process [6]:

$$\frac{1}{2}\Delta\varphi(\omega|\nu) + \rho[\chi^{\mathfrak{p}}_{\Xi} - \varphi(\omega|\nu)] \quad = \quad 0. \tag{10}$$

In this equation, the process is controlled by the 'complexity parameter' ρ given by

$$\rho = \log \|\nu\|.$$

This implies that we can generate the capturing probability $\varphi(\omega|\nu)$ for not-yet-identified imaging process ν only if the associated image $\chi^{\mathfrak{p}}_{\Xi}$ is provided with the guess for the size of unknown set ν. Thus, we can evaluate complex behavior of imaging process (7) within the framework of statistical analysis on the probability space $(\Omega, \mathcal{F}[\Omega], \chi^{\mathfrak{p}}_{\Xi})$.

Generally, roadway patterns in the bird's eye view can be segmented in terms of chained rectangles. Noticing this, let the randomness of the roadway image be generated via the self-similarity process illustrated in Fig. 8. The vestige of the imaging process (7) can be restored as shown in Fig. 9; it is not easy to discriminate complex attractor embedded in random dots (a);

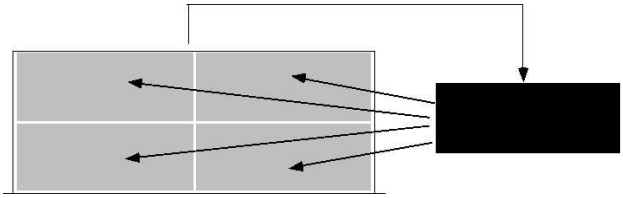

Figure 8: Self-Similarity Process ν

Various patterns can be generated as the attractor of fractal collage process. The bird's eye view of roadway is approximated by a chain of rectangles. Each rectangle can be identified with Sierpinski's carpet: a fractal attractor associated with 4 types of reduced affine mappings.

however, distribution of attractor points can be visualized in terms of the capturing probability $\varphi(\omega|\nu)$ associated with the mapping parameter ν (b); applying invariant test to feature point extracted in the smooth image $\varphi(\omega|\nu)$, the imaging process is verified to generate essentially the same attractor (c).

Due to perspective projection, the roadway patterns are observed as a part of triangle specified in terms of two parameters: width at the foot and vanishing point. Despite the uncertainty of these parameter due to instability of view angle, skewed pattern can be identified with a 'generic' pattern which yields geometrically non-unique view in scene images. As the representation of such generic pattern, consider fractal attractor specified in terms of a set of contraction mappings

$$\nu \quad = \quad \{\, \mu_i, i = 1, 2, 3, 4 \,\},$$

with fixed points

$$\mathfrak{f}_\nu \quad = \quad \left\{\, \omega^f_{\mu_i}, i = 1, 2, 3, 4 \,\right\},$$

as illustrated in Fig. 10. The feature set $\mathfrak{f}_\nu$ should be adapted to generate a view of roadway encountered in observed scene image.

The feature set $\mathfrak{f}_\nu$ is identified on a specific scene by estimating the invariant measure $\chi^{\mathfrak{p}}_\Xi$ on the scene image. For this purpose, the 'frequency shift' due to the perspective projection is extracted in the following gray scale image:

$$\|f\|^{\mathtt{NTSC}} \quad = \quad 0.299\mathtt{R} + 0.587\mathtt{G} + 0.114\mathtt{B}. \quad (11)$$

Let $\|f\|^{\mathtt{NTSC}}_\sigma(\omega)$ be the decomposition of $\|f\|^{\mathtt{NTSC}}$ into the component with scale σ:

$$\|f\|^{\mathtt{NTSC}}_\sigma(\omega) \quad \sim \quad g_\sigma * \chi^{\mathfrak{p}}_\Xi(\omega) + b(\omega), \quad (12a)$$

where

$$g_\sigma(\omega) \quad = \quad \frac{1}{2\pi\sigma^2} \exp\left[-\frac{|\omega|^2}{2\sigma^2}\right],$$

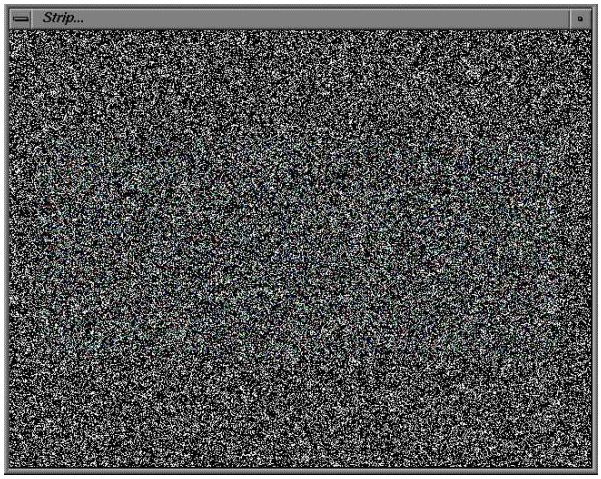

(a) Attractor in Noisy Image

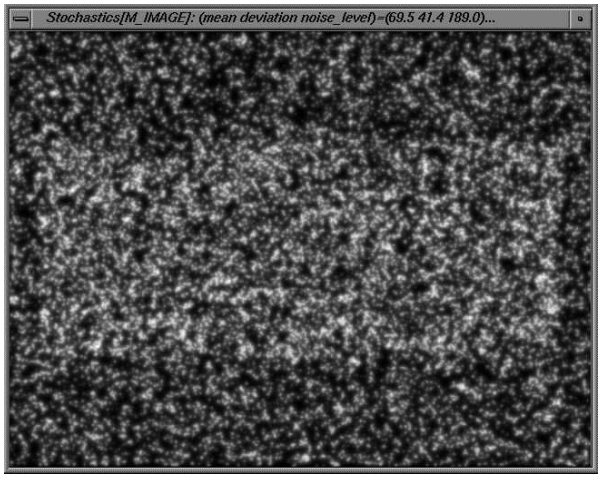

(b) Capturing Probability $\varphi(\omega|\nu)$

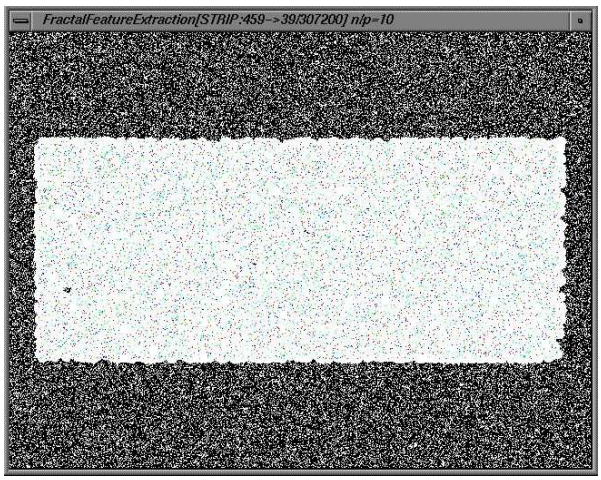

(c) Restoration of Fractal Attractor

Figure 9: Detection of Fractal Imaging Process

Noisy Sierpinski's carpet can be separated from background noise in capturing probability to restore mapping set.

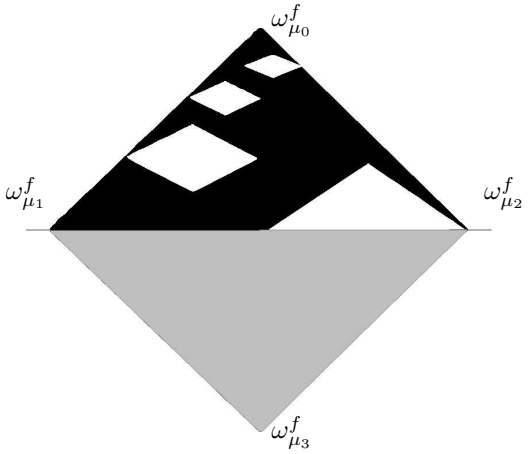

Figure 10: Fractal Representation of Generic Road

Roadway pattern is modeled by rectangle skewed through perspective projection. Skewed carpet can be modeled as a fractal attractor which is observed with random patterns on the surface.

and $b(\omega)$ denotes nonnegative bias satisfying

$$|\Delta b| \quad \ll \quad |\Delta g_\sigma|. \tag{12b}$$

Suppose that the local scale is evaluated in terms of the following biased correlation

$$\sigma^2 \left| \frac{1}{2} \Delta \|f\|^{\mathtt{NTSC}}_\sigma(\tilde{\omega}) \right| \quad \sim \quad \|f\|^{\mathtt{NTSC}}_\sigma(\tilde{\omega}) - b(\tilde{\omega}), \tag{13}$$

where $\tilde{\omega}$, denotes the local maximum point of $\|f\|^{\mathtt{NTSC}}$. Furthermore, we notice that

$$\begin{aligned} \frac{\|f\|^{\mathtt{NTSC}}_{\sigma+\varepsilon}(\omega)}{\|f\|^{\mathtt{NTSC}}_{\sigma}(\omega)} \quad &= \quad \mathfrak{Re}\left[\exp\left[2\pi j \frac{\varepsilon(x+y)}{\sigma(\sigma+\varepsilon)}\right]\right] \\ &\sim \quad \frac{1}{2\pi}\exp\left[-\frac{|\varepsilon|^2}{2}\right], \end{aligned} \tag{14}$$

for $\omega = (x, y)$. With the evaluation (13) an (14), the scale deviation ε conditioned by *a priori* scale model σ can be indexed by the following Gaussian measure g_σ given by

$$g_\sigma \quad = \quad \frac{1}{2\pi}\exp\left[-\frac{|\varepsilon|^2}{2}\right].$$

By introducing the following association

$$\hat{\chi}^{\mathfrak{p}}_\Xi \quad \sim \quad g_\sigma(\varepsilon) g_{\mathtt{RGB}}(\theta_{ij}) \|f\|^{\mathtt{NTSC}},$$

we have the probability for capturing Ξ in observed image $(\Omega, f^{\mathtt{RGB}})$ as the steady state of the following system:

$$\frac{\partial}{\partial t}\varphi_t(\omega|\hat{\nu}) \quad = \quad \frac{1}{2}\Delta\varphi_t(\omega|\hat{\nu}) + \rho[\hat{\chi}^{\mathfrak{p}}_\Xi - \varphi_t(\omega|\hat{\nu})], \tag{15}$$

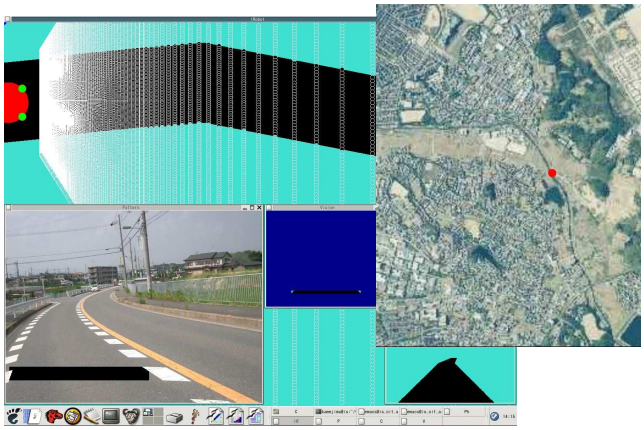

Figure 11: Concept Model

Image processor and robot simulator are integrated for system level simulation of proposed mapping process. Simulated robot is controlled on the roadway model by using road edge sensor which imitate the performance of onboard camera. The roadway model is associated with bird's eye photograph via GPS data.

where $\varphi_t(\omega|\hat{\nu})$, $t > 0$, is convergent sequence of measures conditioned by a mapping set

$$\hat{\nu} \quad = \quad \left\{ \hat{\mu}^f_i, i = 1, 2, 3, 4 \right\}.$$

To detect roadway patterns, generic model illustrated in Fig. 10 is matched with the steady state of the sequence $\varphi_t(\omega|\hat{\nu})$ via the following steps:

- First, select local maximum point of $\hat{\varphi}(\omega|\hat{\nu})$ as stochastic features of generic roadway.
- Next, estimate the direction of the roadway on which the vanishing point $\omega^f_{\hat{\mu}_0}$ should be located.
- Finally, compute the variance of the stochastic features to evaluate the boundary parameter $(\omega^f_{\hat{\mu}_1}, \omega^f_{\hat{\mu}_2})$.

The generic roadway specified in terms of vanishing points and boundaries can be generated as the fractal attractor with the following set of fixed points.

$$\mathfrak{f}_{\hat{\nu}} \quad = \quad \left\{ \omega^f_{\hat{\mu}_i}, \hat{\mu}_i \in \hat{\nu} \right\}.$$

5 SIMULATIONS AND EXPERIMENTS

The schematics of in-process multi-view point integration has been demonstrated via experimental studies. In these experiments, the implications of randomness based image analysis is evaluated on a concept model as shown in Fig. 11; symbolic roadway model is visualized as 'arena' (background) to associate bird's eye view (upper-right) and frontal view (lower-left); positioning results based on two image are fed back to

(a) Detected Segment

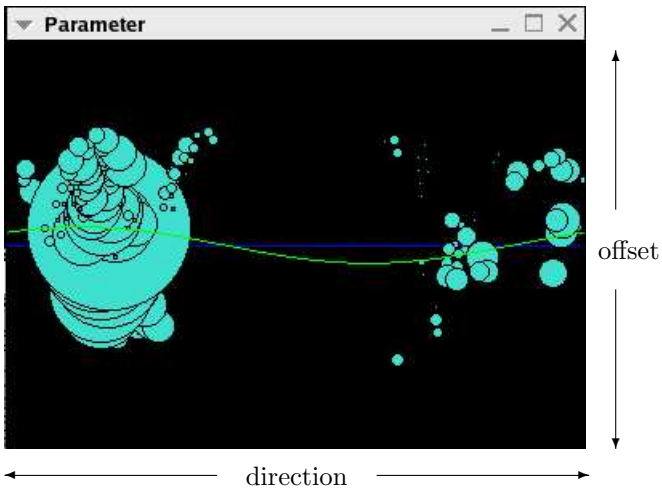

(b) Estimated `(direction offset)` Distribution

Figure 12: Roadway Pattern Detection

In Bird's Eye Imagery, roadway pattern is segmented in terms of chained rectangles. The direction of each rectangle is extracted in a region confined by the estimate of GPS residual by using Hough voting; (origin-direction) pair of the roadway model is specified through the maximization of chromatic consistency index. Detected segment is indicated in local window and, simultaneously, the consistency index of each candidate model is displayed in the direction-offset plane

robot model to shift the location in the arena; onboard sensing processes are simulated on the arena to evaluate the control algorithm and to generate predicted lane (lower-right).

Figure 12 illustrates the results of segment detection in a bird's eye image; for covering positioning error by the GPS residual, the system open a small window in which all possible segments are matched with generic palette to select candidates of the roadway pattern (a); matching results are visualized to evaluate the risk of the segmentation (b). As shown in these results, generic palette can extract chromatic complexity even in considerably diluted observations. By the introduction of the topology indexed by Gaussian measure, the matching allowance is reduced to 1/10 of conventional variance-based classification method.

(a) Scene Image

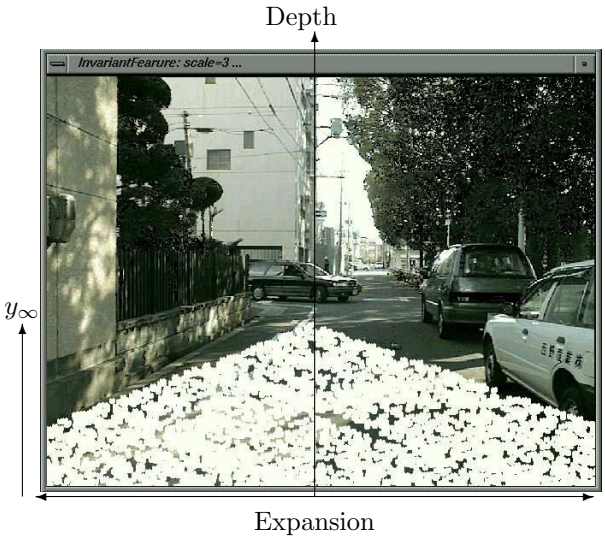

(b) Detected Attractor

Figure 13: Generic Pattern Detection

Invariant measure $\hat{\chi}^{\mathfrak{p}}_{\Xi}$ is estimated based on the evaluation of the scale sift $g_\sigma(\varepsilon)$ and chromatic consistency $g_{RGB}(\phi_i|\mathfrak{s})$. The estimate $\hat{\chi}^{\mathfrak{p}}_{\Xi}$ conveys sufficient information for specifying fixed points $\omega^f_{\mu_i}$ to identify the self-similarity process. Resulted attractor is indicated on the scene image for verification.

Figure 13 shows the results of experiments for identifying generic roadway in complex scene imagery $f^{\mathtt{RGB}}$ as shown in (a); the generic model $\mathfrak{f}_{\hat{\nu}}$ is extracted based on the estimate $\chi^{\mathfrak{p}}_{\Xi} \sim g_\sigma g_{\mathtt{RGB}} \|f\|^{\mathtt{NTSC}}$ (b). These results implies that the introduction of generic palette can reduce the disturbance due to shadow pattern un-

der full daylight. The method was extended to various roadways with complex background and/or random texture successfully.

As the result of these simulations and experiments, the morpho-chromatic randomness was demonstrated to provide significant information for roadway segmentation both in bird's eye and frontal scene imagery. The feasibility of the interactive mapping scheme was verified by prototyping on the concept model. Through test operations, the following requirements for image and signal analysis were clarified.

- GPS with drift correction yields sufficient information for direct coupling of bird's eye and frontal views.
- Piecewise rectangle segmentation provides consistent basis for both prediction and detection of roadway pattern.
- Morpho-chromatic randomness sampled on skewed rectangle attractor restores *as-is* expansion of roadway area.
- Pallet based expansion is sufficiently 'clear' for fractal coding scheme to identify generic roadway model.
- Randomness based coding is insensitive to lighting and coloring noise.
- On the randomness based expansion, we can extract iconic information for tracking sensors to *as-is* roadway pattern.
- By this online-onboard precise tracking, GPS drift is relatively canceled in turn to generate bias-free prediction for obstacle scanning and risk evaluation on generated arena.

6 CONCLUDING REMARKS

It has been demonstrated that real time bindings of satellite/avionics sensors with onboard vision via GPS can afford to support *as-is* basis for autonomous maneuvering. The introduction of piecewise rectangle segmentation integrates bird's eye and frontal views via randomness-based fractal coding of natural complexity. Through simulation and experimental studies, the feasibility of the framework with requirements for image processing was clarified.

References

[1] M. F. Barnsley. *Fractals Everywhere*, Academic Press, 1988.

[2] H. Gardner. *Frames of Mind -The Theory of Multiple Intelligence* -, Basic Books, 1983.

[3] J. J. Gibson. *The Ecological Approach to Visual Perception*, Houghton Mifflin Company, 1979.

[4] H. Helson. Fundamental principles in color vision I: The principle governing changes in hue, saturation and lightness of non-selective samples in chromatic illusion. *J. of Exp. Physiol.*, 23:439–471, 1938.

[5] J. E. Hutchinson. Fractals and self similarity. *Indiana University Mathematical Journal*, 30:713–747, 1981.

[6] K. Kamejima. Stochastic design of imaging parameters for self-similar patterns. *Nonlinear Analysis, Theory, Methods and Applications*, 30:2231–2236, 1997.

[7] K. Kamejima. Chromatic consistency analysis for object identification in noisy scene. In *Proc. ISCIE-SSS'03*, pages 59–64, 2004.

[8] K. Kamejima. Laplacian-gaussian sub-correlation analysis for the extraction of maneuvering affordance in random image fields. In *Proc. IEEE-SEE CSIMTA04*, pages 571–576, 2004.

[9] K. Kamejima. GPS/GNSS residual analysis via competitive-growth modeling of ionosphere dynamics. In *Proc. EUSIPCO05*, pages WedAmOR4–2(4 pages), 2005.

[10] K. Kamejima. Laplacian-gaussian sub-correlation analysis for scale space imaging. *International Journal of Inovative Computting, Information and Control*, 1:381–399, 2005.

[11] K. Kamejima. Kalman filter adaptation on underlying Volterra's principle – estimatable modeling approach to naturally complex systems –. *International Journal of Inovative Computting, Information and Control*, 2:997–1015, 2006.

[12] K. Kamejima, R. Dennert, and Y. C. Watanabe. Open logic machine - an interactive perception architecture for unstructured scene analysis -. *Advanced Robotics*, 8:385–411, 1994.

[13] K. Kamejima, T. Hamada, M. Tsuchiya, and Y. C. Watanabe. From self navigation to driver's associate: an application of mobile robot vision to a vehicle information system. In *Vision-based Vehicle Guidance*. Springer-Verlag, 1992.

[14] K. Kamejima, Y. C. Ogawa, and Y. Nakano. Perception control architecture in image processing system for mobile robot navigation. In *Proc. IEEE-IECON'84*, pages 52–57, 1984.

[15] D. Marr. *Vision – A Computational Investigation into the Human Representation and Processing of Visual Information*, W. H. Freeman and Company, 1982.

[16] U. Neisser. *Cognition and Reality - Principle and Implications of Cognitive Psychology*, Freeman, 1976.

[17] Y. C. Ogawa, K. Kamejima, and Y. Nakano. Syntactic image analysis for environment understanding. In *Proc. IEEE-IWMVI*, pages 266–271, 1987.

[18] PBS/NOVA. The great robot race – what robots see. `http://www.pbs.org/wgbh/nova/darpa/see.html`, 2006.

[19] S. Tsuji. Monitoring of a building environment by a mobile robot. In *Proceedings of the 2nd International Symposium on Robotics Research*, pages 349–356, 1984.